Applying global warming levels of emergence to highlight the increasing population exposure to temperature and precipitation extremes

David Gampe[1], Clemens Schwingshackl[1], Andrea Böhnisch[1], Magdalena Mittermeier[1], Marit Sandstad[2], Raul R. Wood[1,3,4]

[1] Dept. of Geography, Ludwig-Maximilians-Universität München
[2] CICERO Center for International Climate Research, Oslo, Norway
[3] WSL Institute for Snow and Avalanche Research SLF, Davos Dorf, Switzerland
[4] Climate Change, Extremes and Natural Hazards in Alpine Regions Research Center CERC, Davos Dorf, Switzerland

Corresponding author: David Gampe (d.gampe@lmu.de)

Key Points:

- Global warming levels of emergence represent a viable concept to communicate climate change impacts at policy-relevant temperature targets.
- Every fraction of a degree matters as the population exposure to new climate states of minimum and maximum temperatures increases sharply.
- Applying multiple SMILEs to robustly quantify the joint emergence of new climate states and their scaling with global warming.

Abstract

Global temperatures exceeded pre-industrial conditions by 1.1°C during the decade 2011-2020 and further warming is projected by climate models. An increasing number of climate variables exhibit significant changes compared to the past decades, even beyond the noise of internal climate variability. To determine the year when climate change signals can be detected, the concept of time of emergence (ToE) is well established. Additionally, climate projections are communicated increasingly frequently through global warming levels (GWLs) rather than time horizons. Yet, ToE and GWL have barely been combined so far. Here, we apply five Single Model Initial-condition Large Ensembles (SMILEs) to derive global warming levels of emergence (GWLoE) of four temperature and precipitation indices. We show that the concept of GWLoE is particularly promising to constrain temperature projections and proves a viable tool to communicate scientific results. We find that >75% of the global population is exposed to emerged signals for nighttime temperatures at a GWL of 1.5°C, increasing to >95% at 2.0°C. Daily maximum temperature follows a similar, yet less pronounced path. Emerged signals for mean and extreme precipitation start appearing at current GWLs and increase steadily with further warming (~20% population exposed at 2.0°C). Related probability ratios for the occurrence of extremes indicate a strong increase where temperature extremes reach widespread saturation (extremes occur every year) particularly in (sub)tropical regions below 2.5°C warming. These results indicate that current times are a critical period for climate action as every fraction of additional warming substantially increases the adverse effects on human wellbeing.

Plain Language Summary

Climate change represents a major challenge for humankind in the 21st century as human activity has caused and continues to cause global temperatures to rise. However, weather and climate are both characterized by fluctuations that occur naturally even without climate change. We use a special suite of climate models – named Single Model Initial-condition Large Ensembles (SMILEs) – to determine if and also when climate change is detectable beyond these natural fluctuations, that is the time of emergence. The communication of warming targets (e.g., limiting global warming to 1.5°C or 2.0°C) is well accepted and policy-relevant. We therefore translate the time of emergence to the global warming prevalent in the corresponding year of emergence, which then yields the global warming level of emergence. We show that already under the defined warming target of 1.5°C large parts of the global population and land area are confronted with extreme temperatures altered by climate change. This exposure shows a sharp increase for higher global warming levels. Additionally, precipitation starts to show clear climate change effects at 1.5°C – 2.0°C global warming. Our results highlight the urgent need for further climate policies to reduce negative impacts of climate change on human wellbeing.

1 Introduction

The sixth Assessment Report of the Intergovernmental Panel on Climate Change (IPCC) repeatedly confirmed that the recent global warming is unequivocally caused by anthropogenic activity (Masson-Delmotte et al. 2021). The latest decade (2011-2020) saw 1.1°C higher global temperatures compared to pre-industrial times (1850-1900) and warming is projected to continue in the future under current climate policies (IPCC 2022). To prevent adverse and potentially catastrophic impacts of very high warming rates, the Paris Agreement urges to hold global

warming "well below 2.0°C above pre-industrial levels", ideally limiting it to 1.5°C (UNFCCC, 2015). However, a warming of 1.5°C will already impose negative impacts on ecosystems and human wellbeing (Masson-Delmotte et al. 2018), and a growing body of literature highlights the adverse consequences of even higher warming rates (e.g., Hoegh-Guldberg 2019, Schwingshackl et al. 2021). Many studies have elaborated on the benefits of limiting global warming to 1.5°C compared to 2°C, showing, among others, substantially less area affected by desertification (Park et al. 2018), less population exposed to extreme daily temperatures (Harrington,2021, King & Karoly 2017), a lower reduction in water availability and a smaller increase in dry spell length (Schleussner et al. 2016), as well as a less pronounced increase in drought risk and risk of consecutive drought years (Lehner et al. 2017a). Given the current warming rate and the expected severe impacts if exceeding 1.5°C of warming, it is essential to estimate the consequences of warming levels beyond political targets at incremental steps.

The time of emergence (ToE) is a well-established concept to estimate whether and when a climate change signal is detectable (e.g., Lehner et al. 2017b, Hawkins and Sutton 2012). ToE indicates the time when the considered climate variable changes into a new state. This is generally estimated by testing whether the distribution of this variable is significantly different from the distribution that the variable should have in a world without climate change. While expressing ToE in distinct years is illustrative and easy to communicate, uncertainties of climate projections make a precise estimation challenging (Hawkins et al. 2014). Climate projections are subject to three major sources of uncertainty: uncertainty due to internal variability of the climate system, structural uncertainty introduced by different model parameterizations, and scenario uncertainty reflecting differences in potential future socioeconomic and related emission pathways (Hawkins & Sutton, 2009; Lehner et al. 2020). Various methods have been developed to quantify, distinguish and constrain the different types of uncertainty (Lehner et al. 2023).

To disentangle a robust climate change signal from the background noise of internal climate variability Single Model Initial-condition Large Ensembles (SMILEs) are widely used (e.g., Deser et al. 2020, Maher et al. 2021). SMILEs constitute numerous independent, yet equally probable climate simulations, created by running a single climate model multiple times under the same external forcing (e.g., same emission scenario) but with marginally changed initial conditions (Kay et al. 2015, Maher et al. 2019). Due to the resulting large sample size, SMILEs allow for a robust assessment of extremes by extensively sampling the tails of the distribution (Suarez-Gutierrez et al. 2020, Wood et al. 2021). Moreover, SMILEs are ideal tools to estimate ToE due to their ability to provide both statistically robust forced signals and a quantification of internal climate variability via the spread across ensemble members (Schlunegger et al. 2019). This is particularly relevant as internal climate variability can advance or delay the emergence of the forced signal by up to several decades (Hawkins et al. 2014). The increasing number and availability of SMILEs over recent years (Deser et al. 2020) makes it possible to additionally address structural uncertainty. Merging the information of multiple SMILEs to assess the corresponding joint time of emergence should thus allow for an even more robust detection of ToE, as internal variability and model uncertainty can both be assessed.

In recent years, future climate projections have been expressed increasingly frequently through global warming levels (GWLs) instead of fixed time horizons (e.g., the period 2071-2100) (Seneviratne et al. 2021). This approach constrains scenario uncertainty by the question of which GWL will be reached and expresses future climate projections in a more policy-relevant way. Recently, first studies combined GWL and ToE to provide global warming levels of emergence (GWLoE) instead of ToE (Abatzoglou et al. 2019, Kirchmeier-Young et al. 2019,

Raymond et al. 2020). Yet, GWLoE remains a rarely applied concept in general as well as in the context of using SMILEs in particular.

We thus expand the current literature by presenting the joint GWLoE of selected temperature and precipitation indices using multiple SMILEs from the Coupled Model Intercomparison Project Phase 6 (CMIP6) and further aim to promote the concept of GWLoE. We quantify the exposure of population and land area to emerged climate indices as a function of GWL. Further, we relate incremental changes in GWL to changes in the exposure to temperature and precipitation extremes by estimating increases in their probability ratios for each 0.1°C warming.

2 Materials and Methods

2.1 SMILEs and climate indices

We use five different SMILEs from the CMIP6 archive (ACCESS-ESM1-5, CanESM5, EC-Earth3, MIROC6, and MPI-ESM1-2LR; see Tab. 1) with a comparable ensemble size, and sufficient ensemble members (30-50) for representing internal climate variability (Milinski et al. 2020, Tebaldi et al. 2021). A sufficiently large ensemble size is particularly relevant for precipitation variability, for which the ensemble should comprise at least 30 members (Wood et al. 2021). We selected four temperature and precipitation indices compiled by the Expert Team on Climate Change Detection and Indices (ETCCDI) that have been frequently applied in previous studies (e.g. Sillmann et al. 2013, Deng et al. 2022): yearly maximum of daily maximum temperature (TXx), yearly maximum of daily minimum temperature (TNx), total annual precipitation (PRCPtot), and yearly maximum 1-day precipitation (Rx1day). After calculating the indices, all models were remapped using a conservative remapping approach to match the spatial resolution of the coarsest grid (CanESM5, ~2.8°x2.8°; Tab. 1).

We aim at analyzing a wide range of potential GWLs to identify the impact of incremental changes of global warming on selected indices and the related emerging risks. Hence, we selected SMILEs under the historical scenario and the high-end climate change scenario SSP5-8.5, which projects an increase in radiative forcing of 8.5 W/m^2 by the end of the 21st century (Gidden et al. 2019). The choice of this rather extreme scenario allows us to analyze high warming levels (above 3.5°C) compared to pre-industrial conditions (1850-1900; Fig. 1). In contrast, some of the lower emission scenarios might not even reach GWLs of 1.5°C to 2°C by the end of the century despite an already observed global warming of more than 1.1°C in the recent decade (2011-2020; Fig. 1). Overall, the range of GWLs projected by the five selected SMILEs for the end of the 21st century (3.8°C – 7.1°C; Fig. 1) is in general agreement with the full spread of the current CMIP6 climate model ensemble projections (Tebaldi et al. 2021).

Tab.1: Overview of the five Single Model Initial-condition Large Ensembles (SMILEs) applied in this study. The CMIP6 historical and SSP5-8.5 scenarios (in total covering the period 1850-2100) were considered for all SMILEs. All models were conservatively remapped to the coarsest model grid (CanESM5) for further analysis. The values for Equilibrium Climate Sensitivity (ECS) stem from Meehl et al. (2020) and provide an estimate of the climate sensitivity of each SMILE.

SMILE	**Ensemble size (n members)**	**Original resolution (lat x lon grid)**	**ECS (°C)**	**Reference**

ACCESS-ESM1-5	40	~1.3°x1.9°	3.9	Mackallah et al. 2022
CanESM5	50	~2.8°x2.8°	5.6	Swart et al. 2019
EC-Earth3	50	~0.7°x0.7°	4.3	Wyser et al. 2021
MIROC6	50	~1.4°x1.4°	2.6	Tatebe et al. 2019
MPI-ESM1-2LR	30	~1.9°x1.9°	3.0	Mauritsen et al. 2019

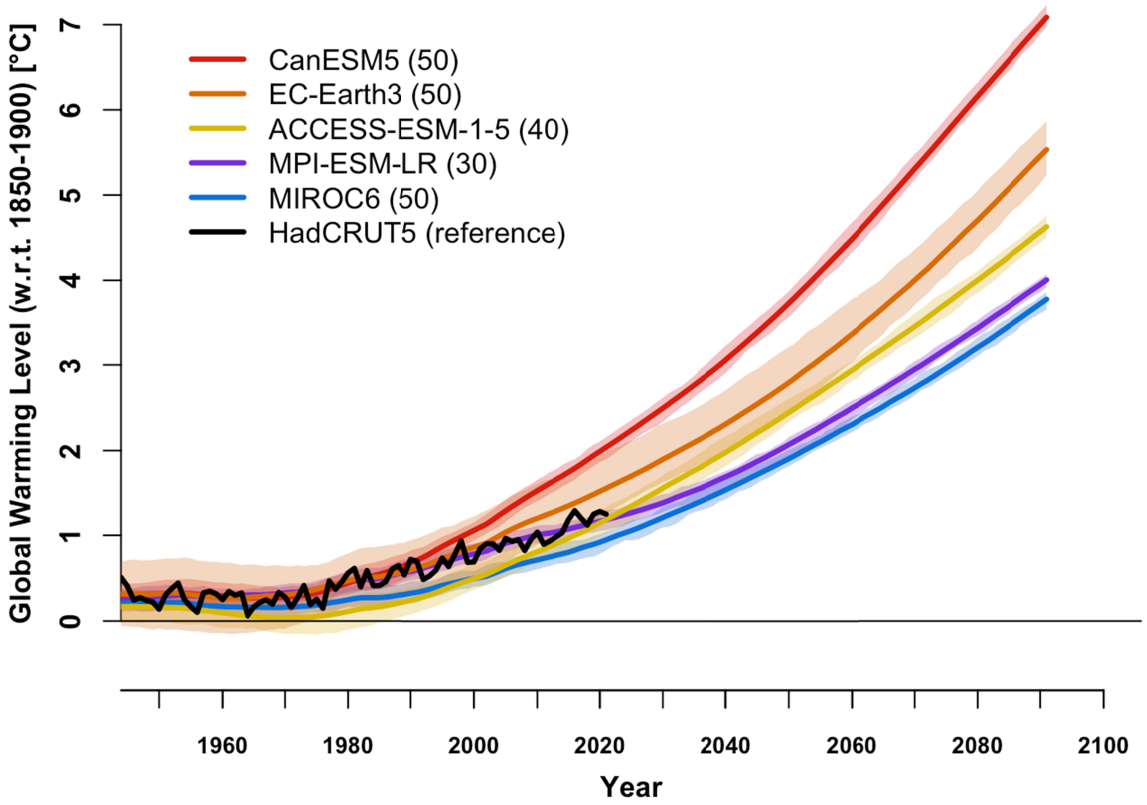

Fig. 1: Changes in global average annual surface air temperature, i.e., Global Warming Level (GWL). GWL was calculated relative to pre-industrial conditions (1850-1900) under historical and SSP5-8.5 scenarios and is presented for the five SMILEs (colors indicate their respective equilibrium climate sensitivity (ECS) from low (blue) to high (red)) and the blended, observation-based reference data set HadCRUT5 (black; Morice et al. 2021). Solid lines indicate the ensemble mean and shaded areas represent the range (minimum-to-maximum) of the individual members for each SMILE. Numbers in the legend indicate the ensemble size of each SMILE (n members).

2.2 Time of Emergence (ToE) and Global Warming Level of Emergence (GWLoE)

To calculate ToE, we extract 20-year moving windows for each year over the period 1901 to 2100 and test the resemblance to the reference climate state (pre-industrial period, 1850-1900) using a two-sided Kolmogorov-Smirnov test (KS-test) at 5% significance level (Mahlstein et al. 2012, King et al. 2015). The climate signal is considered as emerged once the KS-test indicates

that the tested time series was drawn from a different distribution than the reference data. For each ensemble member, we define ToE as the tenth year of the first 20-year window where the p-value of the KS-test determines significance in changes in the mean. We further require that changes in the mean of all subsequent periods remain significant as well. The climate signal is considered as not emerged by the end of the 21st century if the KS-test for the last 20-year window (2081-2100) does not yield significant differences. The calculations are carried out for each index and each SMILE member on the grid cell level. The ToE of a given SMILE is then assigned to the year when at least 90% of the ensemble members show emerged climate signals (similar to Martel et al. 2018).

To transfer ToE into Global Warming Level of Emergence (GWLoE), we calculate GWL as the change in the area-weighted global average annual surface air temperature (GSAT) in each moving 20-year window relative to the pre-industrial period following the approach by Hauser et al. (2019) as used in IPCC AR6 (Seneviratne et al. 2021). The GSAT changes are assigned to the tenth year of each 20-year period and define the GWL for that year in each member of each SMILE. The GWL of a SMILE is defined as the mean across all ensemble members (i.e., the forced response). To derive GWLoE, we assign the corresponding GWL to the previously calculated year of climate signal emergence (ToE), thus replacing the time axis with GWL.

To further increase the robustness of the GWLoE estimates, we calculate the joint emergence of the climate signal across all five SMILEs, defined as the median GWLoE of the five SMILEs, for each index at the grid cell level. We additionally conclude that SMILEs agree in signal emergence if at least four SMILEs indicate an emergence within the 21st century. Finally, we cap the GWLoE at 4°C as not all SMILEs reach that warming level by 2100 (Fig. 1).

2.3 Exposure of Population and Land Area to Emerged Climate Signals

For each of the four climate indices (TXx, TNx, PRCPtot, Rx1day), we quantify the fraction of population and the land area fraction affected by emerged climate signals. We use historical population data from ISIMIP2b (Frieler et al., 2017) and future population scenarios according to the different SSPs (SSP1-SSP5; Jones & O'Neill, 2016, Samir & Lutz, 2017). For each of these datasets we calculate the population density and remap it to the coarsest common grid (CanESM5 grid; see Section 2.1) using conservative remapping. As SSP population data are available in 10-year intervals we interpolate linearly in time to obtain yearly resolution. To estimate the time-dependent population exposure to emerged climate signals the population of all respective grid cells are aggregated. We express the result as percentage of (time-dependent) global population. Similarly, we calculate the fraction of global land area, on which a climate signal emerges, using the (time-invariant) land area fraction of CanESM5. The exposures of population and land area to emerged climate signals are finally expressed as a function of GWL.

2.4 Changes in Probability Ratio of Climate Index Extremes

We further quantify how the probability of extreme values of the four climate indices changes with global warming. We define extremes as the 95th percentile (equivalent to a return period of 20 years of high temperature and heavy precipitation events; conceptual Supplementary Fig. S1a) of the corresponding climate index distribution in the reference period 1850-1900. To estimate how extremes alter with global warming, we calculate the change in probability ratio PR for each 20-year period given by

$$(1)\ PR = \frac{\frac{n_{fut}}{y_{fut} \cdot m_{fut}}}{\frac{n_{ref}}{y_{ref} \cdot m_{ref}}}$$

where n is the event frequency during the reference (*ref*) and future (*fut*) periods pooled across all members, y the period length (20 years for *fut*, 51 years for *ref*) and m the number of ensemble members. Probability ratios above (below) 1 indicate an increase (decrease) in event occurrence relative to the reference period 1850-1900. By definition, the occurrence probability equals 0.05 in the reference period when considering the 95th percentile threshold. Therefore, the theoretical maximum probability ratio is *PR=20* and indicates that pre-industrial thresholds are exceeded every year in every SMILE member. We examine the GWL of this saturation effect for the four selected extreme indices with respect to the defined 20-year return periods. Furthermore, to derive the change in probability ratios as a function of GWL we linearly regress the probability ratio against GWL using the least-squares approach. We account for scaling that is not constant across the considered GWL range by performing the linear regression piecewise for three global warming intervals: 1°C to 2°C, 2°C to 3°C, and 3°C to 4°C (see conceptual Supplementary Fig. S1b). The estimated regression coefficients indicate how strongly the probability ratios change with every tenth of a degree (0.1°C) of additional global warming. To account for inter-SMILE differences, we average the regression coefficients, weighted by the number of SMILE members, and mask out areas where less than four model agree in the direction of PR change.

The 0.1°C GWL step we apply is finer than the steps used by other studies to investigate frequency changes at distinct GWL thresholds (e.g., GWLs of 1.5°C or 2.0°C related to the Paris Agreement). Those studies commonly employ distinct GWLs or increments of 0.5°C or 1°C to obtain statistically robust change signals (Perkins-Kirkpatrick & Gibson 2017; King et al. 2018; Fischer & Knutti 2015). However, our setup with five SMILEs, each based on 30-50 ensemble members (220 members in total), ensures robust assessments also at finer incremental GWLs. Analyzing GWL steps of 0.1°C allows us to evaluate the contribution of incremental warming steps to increases in extreme event frequency with particular focus on different warming intervals.

3 Results

3.1 Global warming level of emergence for temperature and precipitation indices

The joint emergence of the four considered indices (TXx, TNx, PRCPtot, and Rx1day) across all SMILEs shows distinct patterns in terms of GWLoE (Fig. 2). In particular, the temperature indices show widespread emergence at low GWLs with substantial emergence occurring at present-day GWL, indicating that many regions have already transitioned into a new climate state for the corresponding index. Emergences of TXx are particularly prevalent in the Southern Hemisphere, including large parts of Africa and South America, as well as Southern Europe, Central America, and the Arabian Peninsula (Fig. 2a). In all other regions, TXx is projected to emerge between a GWL of 1.0°C and 2.0°C except for a few small regions showing emergences only at higher GWLs. TNx shows even more widespread emergence at present-day warming with almost all regions showing emergence at 1°C (except Antarctica), reflecting that climate

246 change has already impacted the temperature indices across the globe (Fig. 2b). The model
247 agreement for the emergence of the temperature indices is very high (no areas are hatched in Fig.
248 2a, b). While the joint emergence of all SMILEs provides an estimate of GWLoE based on the
249 median GWLoE across the five SMILEs, individual models emerge at lower or higher GWLs.
250 Thus, the range of GWLoE across SMILEs provides additional information on the robustness of
251 the results. The robustness is particularly high for TNx, as indicated by a narrow range of
252 GWLoE across SMILEs (Supplementary Fig. S2). While the range yields a generally high
253 agreement also for TXx, the patterns are more diverse, manifested by a larger range in eastern
254 North America, eastern Europe, Central Africa and parts of South America (Supplementary Fig.
255 S2).
256 The precipitation indices emerge over smaller areas and at higher GWLs than the
257 temperature indices (Fig. 2c, d). PRCPtot emerges at a GWL of around 2°C in the Northern high
258 latitudes, central Asia, and parts of tropical Africa and South America (Fig. 2c). For these
259 regions, a general increase in annual precipitation is projected, except for South America (IPCC,
260 2021). Rx1day is generally projected to increase over land due to dynamical and
261 thermodynamical adjustments (Seneviratne et al. 2021). However, the Rx1day signal only
262 emerges in parts of Africa and South America for GWL <2.0°C (Fig. 2d). For the rest of the
263 globe, PRCPtot and Rx1day do not emerge until a GWL of 3°C or higher, with some areas
264 (particularly desert regions) showing no emergence in the data sets at all. In addition to high
265 internal variability, the inter-model range in GWLoE for precipitation indices is larger than for
266 temperature indices, partly explaining that the precipitation indices only emerge at higher GWLs
267 (Supplementary Fig. S2). Regions with a narrower GWLoE range predominantly correspond to
268 grid cells where the signals emerged in less than four SMILEs (North America, the
269 Mediterranean, southern Africa and Australia). The narrow range in these regions is thus based
270 on a smaller SMILE sample and does not necessarily indicate increased robustness.

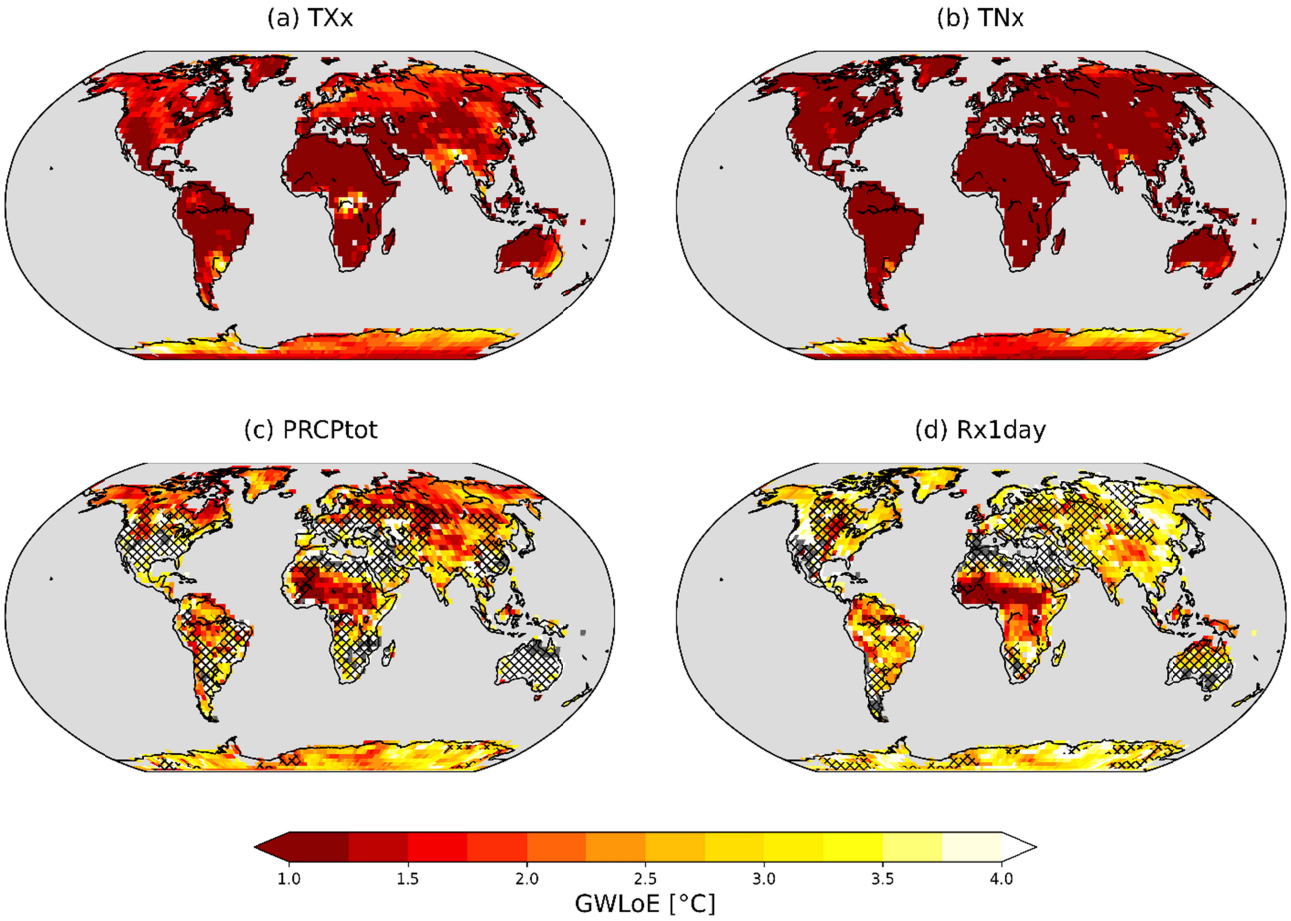

Fig. 2: Joint Global Warming Level of Emergence (GWLoE) of the considered indices. Maps show the joint emergence (multi-model median) of the five applied SMILEs using historical and SSP5-8.5 scenarios for TXx (a), TNx (b), PRCPtot (c), and Rx1day (d). Red colors indicate an earlier emergence. Hatched areas indicate regions where emergence within the considered GWL range was detected in less than four of the five SMILEs. Grid cells that did not yield emergence at GWL<4°C are colored white. No data is shown in dark grey, non-land grid cells in light grey.

3.2. Exposure of land area and population to emerged climate signals

To quantify how the spatial extent of the emerged climate signals changes over time, we next assess the percentage of land area exposed to emerged climate signals as a function of GWL (Fig. 3). Here, TXx has already emerged on 35-55% (range across all SMILEs) of the global land area under present-day climate (GWL = 1.1°C). The emergence continues to increase linearly until stabilizing around 2°C when most of the land fraction (70-90%) shows emerged signals (Fig. 3a). Africa and South America can be identified as hotspots where TXx has emerged already under present-day climate (Supplementary Fig. S3). TNx shows a similar path as TXx. However, most of the land area has already experienced emerged climate signals under present-day conditions (60-80%; Fig. 3b and Supplementary Fig. S3). At a GWL of 1.5°C, 80-90% of the land area will be exposed to a new climate state for TNx (Fig. 3b).

The emergence of climate signals for the two precipitation indices occurs at higher GWLs than for the temperature indices and thus emergences only occur over a small portion of the land area under present-day climate (1-7%; Fig. 3c, d). The fraction of land exposed to PRCPtot emergence shows a linear increase from 1.0°C onwards, with roughly a fifth (15-25%) of the land area being exposed to a new climate state at a GWL of 2.0°C (Fig. 3c). However, we find strong regional differences with emerged signals at 2.0°C warming being more widespread in North & Central Asia, South America, and Africa than on global average (Supplementary Fig. S3). Particularly in North & Central Asia, the estimated exposed land fraction also shows substantial differences across the five SMILEs. The fraction of land exposed to Rx1day emergences also increases linearly, starting at a GWL of around 1.0°C, but the rate of increase depends strongly on the considered SMILE. Three of the five SMILEs (MPI-ESM1-2-LR, MIROC6, and ACCESS-ESM1-5) follow a similar path (around 11-13% of exposed area at a GWL of 2.0°C), while EC-Earth3 shows a much higher exposed area (22%) and CanESM5 a much lower exposed area (4%) at 2.0°C.

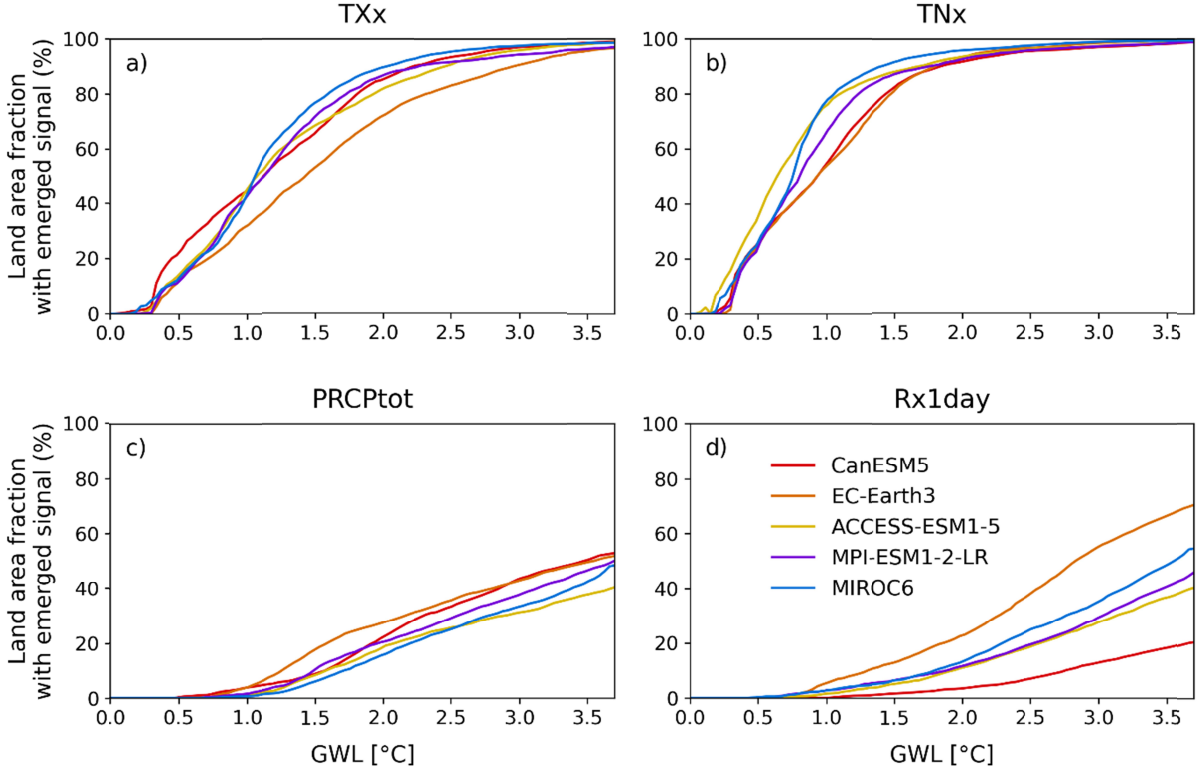

Fig. 3: Fraction of land area exposed to emerged climate indices in dependence of global warming level (GWL). The respective land area fraction is presented for emerged signals of TXx (a), TNx (b), PRCPtot (c), and Rx1day (d). Different colors represent the five applied SMILEs (with equilibrium climate sensitivity (ECS) increasing from blue to red).

We further estimate the percentage of global population that is exposed to emerged climate signals considering the different population scenarios SSP1 to SSP5 (Fig. 4). In general, the patterns of population exposure are similar to the patterns of land area exposure, with large shares of the global population being affected by emergences of TXx and TNx at low GWLs. In contrast, PRCPtot and Rx1day will emerge at higher GWLs and consequently affect fewer people. For TXx, the exposure under present-day climate shows a rather large spread (affecting 35-65% of global population) but converges towards 100% under higher GWLs (Fig. 4a). Regarding TNx, already 60-85% of the global population is exposed to emerged signals under present-day climate, with model agreement being higher than for TXx (Fig. 4b). This percentage is projected to increase to 75-95% at 1.5°C, and at 2.0°C almost the entire population (more than 95% in four out of the five SMILEs) will be exposed to a new climate state of TNx (Fig. 4b). Under present-day warming the highest exposure to TNx emergence can be found in North America, Central & South America, Africa, and Europe where more than four out of five people already experience an emerged climate signal for TNx (Supplementary Fig. S5). For PRCPtot we find lower exposure where up to a GWL of 2.0°C only a small but steadily increasing fraction of the population (5-16%) will experience a new climate state for PRCPtot (except for MPI-ESM1-2-LR, which yields larger fractions). For Rx1day, the exposed population starts to steadily increase at a GWL of 1.0°C but remains below 20% up to 2.0°C. The projections of the different SMILEs diverge at higher GWLs with EC-Earth3 showing the largest and CanESM5 the smallest increases. Particularly pronounced increases in exposure to Rx1day are found in South America and Africa (Supplementary Fig. S5).

The different population scenarios of the SSPs only play a secondary role for the projected fraction of population exposed to emerged signals. For TXx and TNx, the differences across models clearly dominate the uncertainty of the exposed population (Fig. 4a, b) and the population scenario only slightly influences the results. Similarly, for PRCPtot and Rx1day differences across models also dominate but the population scenarios also partly influence the projected exposures (Fig. 4c, d). In particular, a population development following SSP1 leads to substantially lower population exposure to emergences of PRCPtot and Rx1day compared to the other SSPs. This is evident for all SMILEs despite differences in the GWL range where this effect is most pronounced.

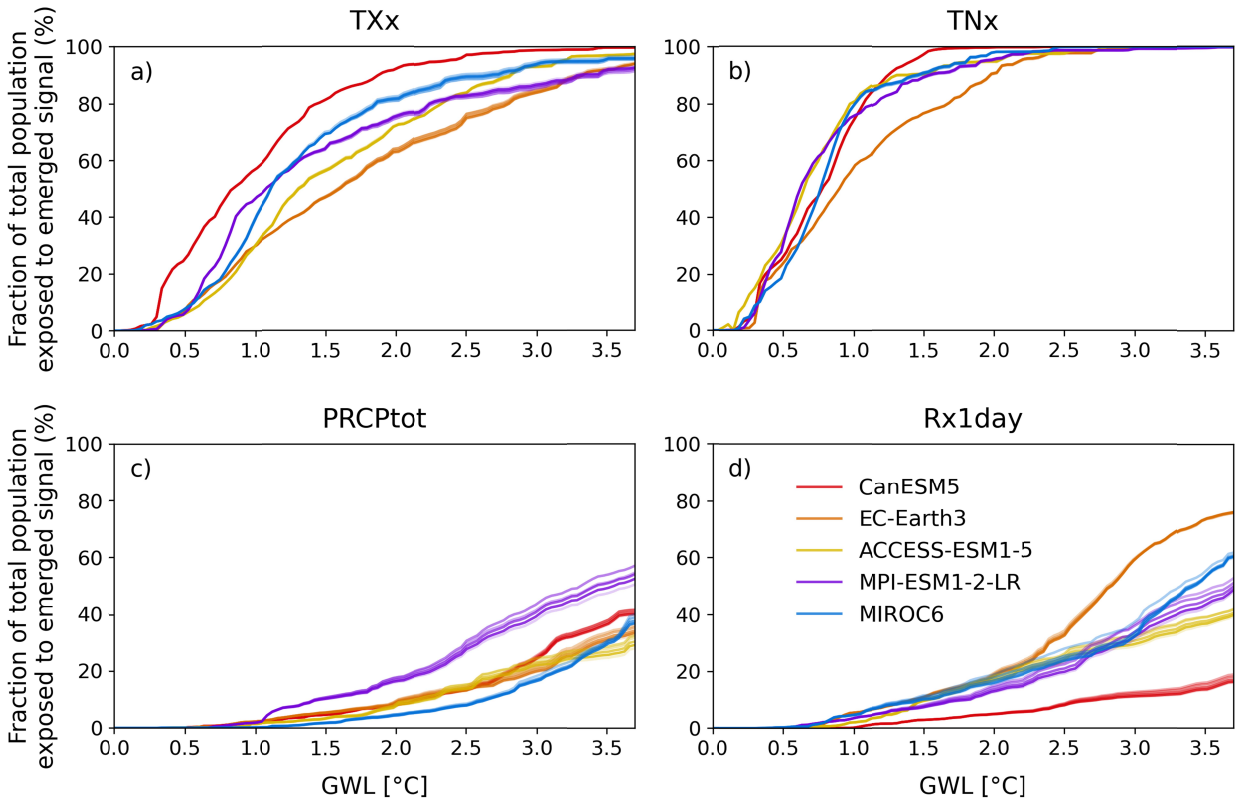

Fig. 4: Percentage of global population exposed to emerged climate indices as a function of GWL. The respective exposed population fraction is presented for emerged signals of TXx (a), TNx (b), PRCPtot (c), and Rx1day (d). Different colors represent the five applied SMILEs (with equilibrium climate sensitivity (ECS) increasing from blue to red). Shading reflects the respective population scenario ranging from SSP1 (dark colors) to SSP5 (light colors).

3.3 Increase in probability ratios for different global warming levels

Next, we investigate how the occurrence of extremes in the four climate indices changes in dependence of GWL by examining differences in their probability ratios relative to pre-industrial conditions (see Methods for details). The temperature indices show a widespread increase in the frequency of extreme events (positive changes in the probability ratio) across all continents in the GWL range 1-2°C (Fig. 5). The increase in the probability ratios of TXx and TNx is largest in central North America, South America, the Mediterranean, and central Asia, with more pronounced increases for TNx than for TXx. In these regions the probability ratio increase per 0.1°C warming is larger than 1. Thus, every additional 0.1°C global warming leads to an increase in the extreme event occurrence by at least the number of events in the pre-industrial reference period (see Methods). Furthermore, the increase in probability ratios of TXx and TNx indicates a non-linear behavior. Largest increases are found in the GWL range of 1-2°C but increases get lower once the peak of the index distribution crosses the defined threshold for extreme events (95% percentile in 1850-1900) and stabilize towards higher GWLs (3-4°C or even higher). The probability ratio patterns remain similar also for a more extreme threshold (99th percentile, corresponding to a 100-year return period), albeit yielding higher increase rates given the lower number of events in that case (Supplementary Fig. S7).

The changes in probability ratio of PRCPtot and Rx1day are generally less pronounced than for TXx and TNx (Fig. 5). They increase by 0.25 to 0.75 per 0.1°C (corresponding to 25-75% higher probability of extreme events per 0.1°C warming) in the northern high latitudes,

Africa, the Himalaya region, and – for Rx1day – parts of South America. These regions also emerge as hotspots for even more extreme events (99th percentile; Supplementary Fig. S7). For PRCPtot, several regions show a decrease in the probability ratio of down to -0.25 per 0.1°C warming (Central and South America, southern Africa, the Mediterranean region, and parts of Australia), indicating a decrease of precipitation in these regions in line with findings of the recent IPCC report (IPCC, 2021). Regions with decreasing probability ratio show lower model agreement than regions with increasing probability ratio. In contrast to the temperature indices, the change patterns of probability ratio for PRCPtot and Rx1day remain similar across GWL ranges, indicating that they are less dependent on the state of global warming.

In several regions probability ratios level off at high GWLs (Fig. 5), indicating that the maximum possible exceedance probability is reached. This GWL of saturation is generally much lower for TXx and TNx (Fig.6), with saturation being reached below 2°C in South and Southeast Asia, and large parts of Africa and tropical South America. Parts of North America and northern Australia reach saturation between 2°C and 3°C (Fig. 6). In contrast, the precipitation indices (PRCPtot and Rx1day) reach saturation in much fewer grid cells and at much higher GWLs, with the Mediterranean, and parts of South America being the only regions reaching saturation for PRCPtot.

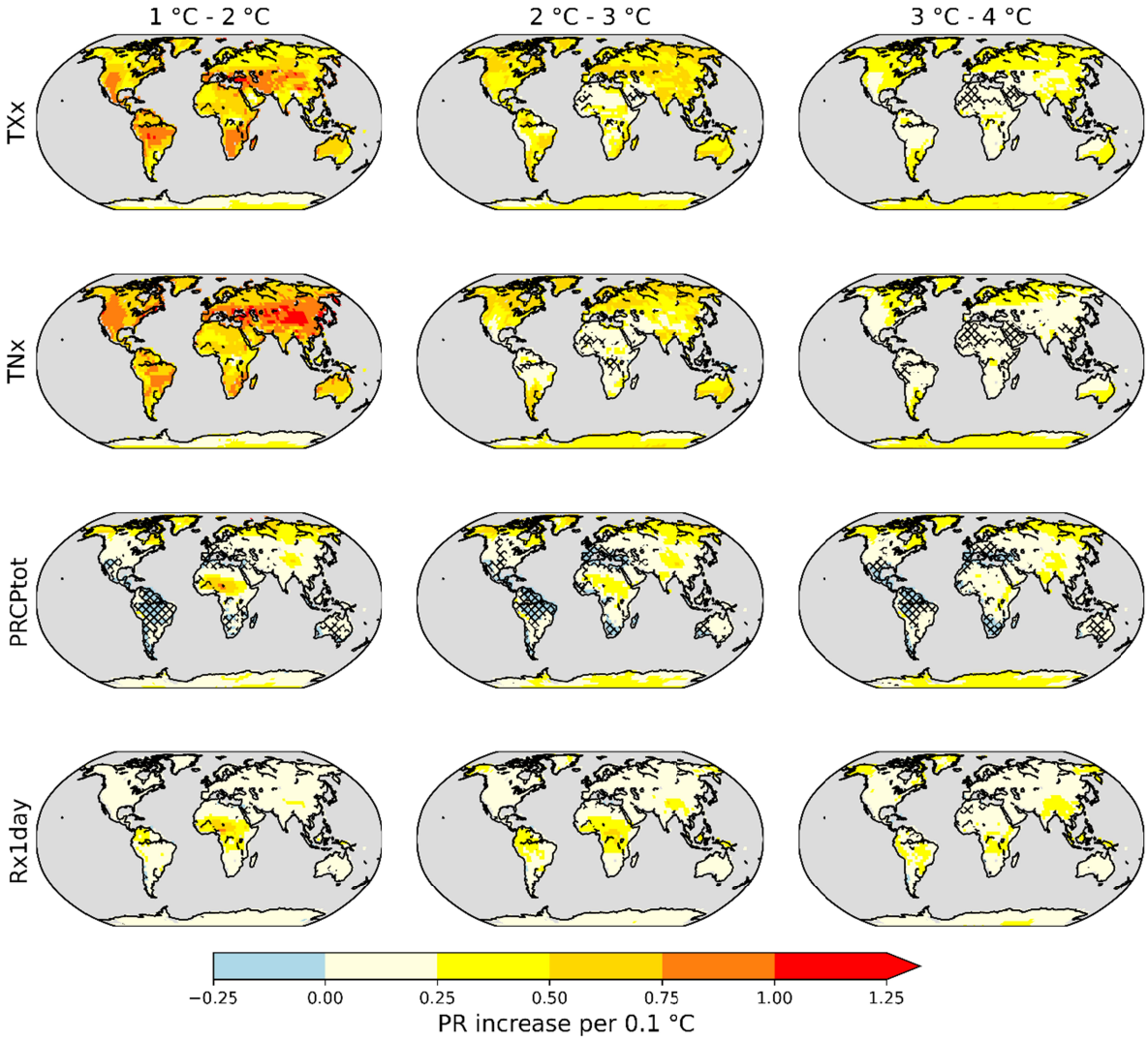

Fig. 5: Probability ratio (PR) increase for extremes in TXx, TNx, PRCPtot, and Rx1day for three ranges of global warming (1°C – 2°C, 2°C – 3°C, and 3°C – 4°C) per 0.1°C warming with respect to 1850-1900. PRs are calculated as the change in exceedance of the 95th percentile of the index distribution in 1850-1900. Yellow-to-red colors indicate increasing PRs, while blue colors indicate decreasing PRs. Hatched areas indicate regions with low model agreement (at least 1 SMILE disagreeing in the sign of PR).

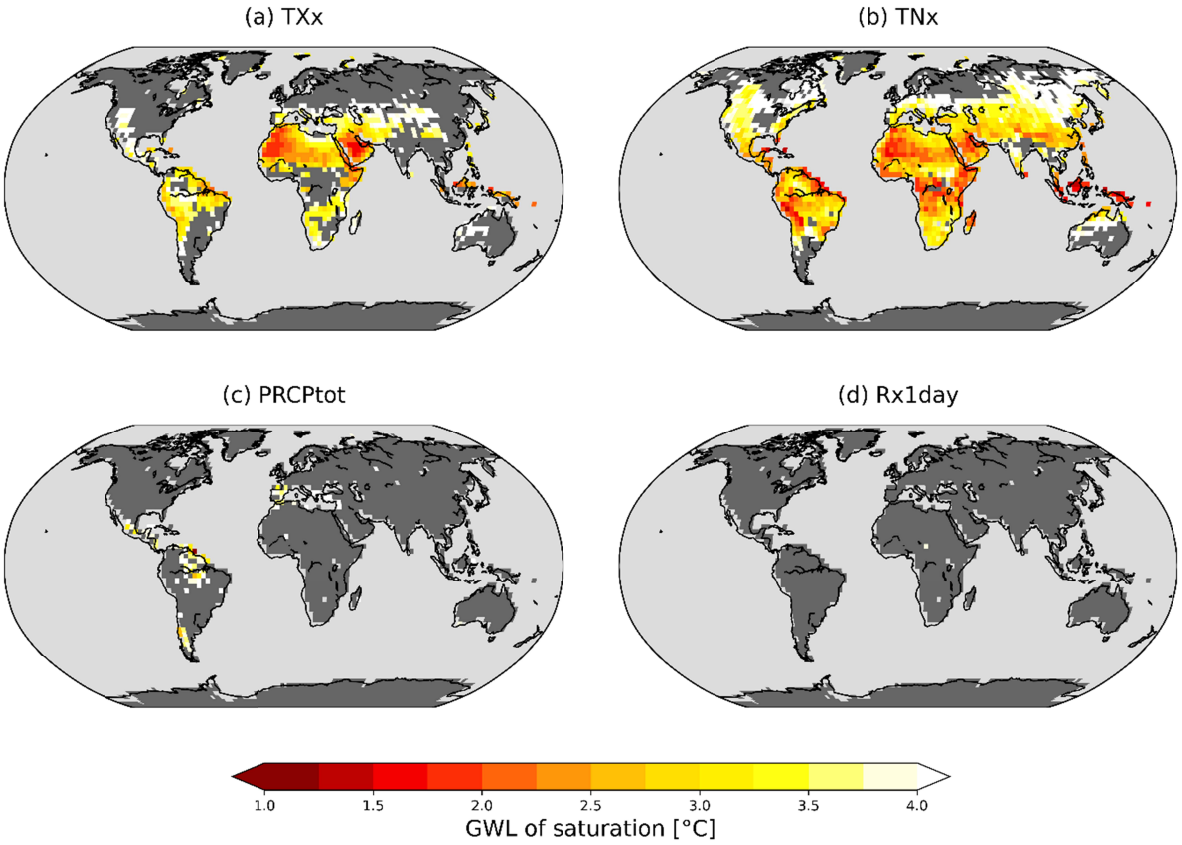

Fig. 6: Global warming level (GWL) of saturation for extremes of the selected indices. Saturation maps for TXx (a), TNx (b), PRCPtot (c), and Rx1day (d) based on values exceeding the 95th percentile of the index distribution in 1850-1900. Saturation is defined as the GWL where the maximum number of extreme events in the analyzed 20-year periods is reached (i.e., 20 out of 20 years), i.e., each year is an extreme year relative to pre-industrial conditions. The values indicate the ensemble median across all SMILEs if at least 4 out of 5 SMILEs show saturation values. Grid cells that indicate joint saturation at higher GWL within the considered spectrum (Fig. 1) are colored white Areas that show saturation in less than 4 of 5 SMILEs are colored in dark grey, non-land grid cells in light grey.

4 Discussion

4.1 Adverse impacts of incremental GWL changes

Our results highlight that incremental GWL changes (i.e., steps of 0.1°C) can strongly increase the emergence of new climate states for the investigated indices. This is particularly the case for temperature extremes (TXx and TNx), for which we find widespread emergence already under present-day GWL. This finding is in line with the increasingly frequently observed heat extremes throughout the world that can be attributed to climate change (Ciavarella et al. 2021, Philip et al. 2022, Philip et al. 2023). The widespread emergence of TNx under current climate conditions is of particular concern, as it corresponds to elevated nighttime temperatures, which can reduce people's recovery potential and may thus weaken their health conditions (Royé et al., 2021, Thompson et al., 2022). At the same time, the precipitation indices Rx1day and PRCPtot start to emerge in the GWL range 1-2°C. This indicates that we are currently in a crucial period, where every fraction of a degree of additional warming may cause further regions to transition into new

climate states. Limiting global warming to 2.0°C would keep the population and land fraction exposed to emergences of Rx1day and PRCPtot below 20%. Beyond 2.0°C the exposure to emergences of these indices will rapidly increase. The current policies, which put the world on track to reach a warming of 2.8°C (Liu & Raftery, 2021), would thus expose a considerable fraction of population and land to new precipitation regimes and most of the population and land area to new temperature regimes (Supplementary Fig. S3 & S5) potentially outside the human climate niche (Lenton et al. 2023). Additionally, the spatial patterns of exposure rates and the frequency of future extremes show a strong regional heterogeneity, which might lead to increased socioeconomic inequality, especially in poorer regions of the world (King & Harrington, 2018).

4.2 Non-linearities and saturation of probability ratios

The responses of precipitation and temperature extremes to global warming appear to follow a non-linear path (Fig. 3 & 4). However, this does not directly speak to the linear or non-linear growth of extremes. Rather, in each grid cell the distribution of a given variable crosses the threshold of emergence at a distinct GWL (schematic Supplementary Fig. S1a). The contribution of this grid cell to the fraction of emerged land is zero before the crossing, and equal to the fractional area of the grid cell afterwards. This continues simultaneously across all grid cells, forming the distribution of emerged grid cells in dependence of the GWL. The increase in emerged land fraction (or population) is particularly steep until the majority of grid cells passed the threshold and flattens out afterwards. Once the thresholds are exceeded in all grid cells, the fraction of emerged grid cells reaches 100% and can no longer increase.

Our results show a very rapid initial growth (i.e., a large fraction of grid cells emerge at similar GWLs) particularly for TNx and (slightly less pronounced) for TXx, in line with saturation patterns corresponding to the non-linear growth seen for CMIP5 models (Fischer & Knutti, 2015). For precipitation, the fraction of emerged land increases more slowly, in line with a more linear growth as seen also in the CMIP5 results of Fischer & Knutti (2015). The respective trajectories of precipitation and temperature extremes are nevertheless alarming. First, the sharp increase of emerged temperature extremes will strongly increase the human exposure to extremely hot temperatures. Second, regional preparedness to future temperature events might be insufficient in case of unexpectedly rapid changes in the occurrence of extremes (King et al. 2018). The usage of small GWL increments (e.g., 0.1°C as used in this study) thus seems imperative, as an assessment across large increments (e.g., 0.5-1.0°C) might undersample the temperature axis and potentially mask changes in the slope of the underlying distribution.

Probability ratios of the temperature indices increase considerably up to a GWL of 2.0°C with widespread saturation reached at a GWL of 2.0°C. This would imply unprecedented heat conditions in Southern Asia, northern Africa, and northern South America for most years even if the 2.0°C target of the Paris Agreement was met (Fig. 5). Precipitation indices reach saturation only at higher GWLs, which points towards more inert adjustments of precipitation to changing climate. It is important to emphasize that the interpretation of saturation levels (which are reached in widespread regions particularly for temperature indices) should not be overly generalized. They are subject to the considered index and the related distribution and additionally depend on the applied threshold (here 95^{th} percentile; see Supplementary Figs. S8-S10 for other percentiles) and the defined reference period (here pre-industrial conditions) (Harrington & Otto, 2018). Considering this though, they can be used as a tool to indicate that events considered "extreme" under pre-industrial conditions occur on a yearly basis once saturation occurs and thus

become the new normal state. Reaching the saturation level of exceedance, however, should not be confused with reaching a 'safe' state and does not impede further changes in the magnitude and intensity of extremes (Harrington & Otto, 2018). Instead, the exceedance of greater extremes (i.e., higher thresholds) likely continues to rise and even hotter temperatures and heavier precipitation events are expected to occur at higher GWLs (Supplementary Fig. S1a).

4.3. Dependence of climate signal emergence on remapping sequencing

To combine and display climate data with different spatial resolution, remapping is essential. In this study, we remapped the data to the grid of the coarsest model (CanESM5) *after* calculating the climate indices (TXx, TNx, PRCPtot, Rx1day). This sequencing takes advantage of model diversity by preserving the precipitation and temperature fields of the models with higher spatial resolution when calculating the indices. It yields a local representation of the considered extreme indices, similar to what observational data sets would deliver (de Vries et al. 2023). Alternatively, climate data can be remapped *before* calculating the climate indices. This sequencing would lead to more harmonized model results but removes the fine scale information provided by models with higher spatial resolution. For studies analyzing model performance and focusing on model comparison, the latter approach would be preferable.

The impact of the processing order on the resulting fields is expected to be more substantial for daily precipitation extremes (such as Rx1day) than for temperature or total annual precipitation. When these precipitation extremes are calculated on the individual grid cells of the finer grid, they might occur on different days and would then be aggregated to form the larger grid cells of the remapped data. Regridding *before* the calculation of the extreme indices would keep the time integrity but results in a dilution of the precipitation extremes that often occur more locally.

For our study, the former approach (remapping *after* calculating the indices) is advantageous, as we aim to investigate local emergences of climate change signals and the related exposure of population. Moreover, we focus on relative changes in the indices (assessed via ToE, GWLoE, PR) rather than changes in their absolute values. We find only negligible difference between both remapping orders for TXx, TNx and PRCPtot for the land area fraction exposed to emerged signals (Supplementary Fig. S11 & S12). However, we identify a substantial divergence for the emergence of Rx1day. Focusing on local level extremes (remapping *after* calculating Rx1day) yields earlier Rx1day emergences compared to the approach that harmonizes model results (remapping *before* calculating Rx1day). Additionally, the latter approach reduces the model spread in case Rx1day emergences are expressed as function of GWL (Supplementary Fig S12), while the spread remains unchanged if emergences are expressed as function of time (Supplementary Fig. S11). This indicates that most of the model spread for Rx1day emergences expressed as function of GWL can be explained by model resolution, whereas the different ECS seems to play a secondary role (Fig. 3d, Supplementary Fig. S12d, Tab. 1). The high sensitivity of ToE/GWLoE for Rx1day (and presumably also for similar precipitation indices) to the selected remapping order highlights that this sequencing is of great importance for quantifying related emergences. The decision on performing the remapping *before* or *after* the calculation the desired index should thus always be tailored to the focus of the

study. Our results highlight that this is crucial not only for the investigation of changes in absolute values but also when ToE or GWLoE are of interest.

4.4 The concept of GWLoE as a tool to communicate climate change impacts

Combining the concept of time of emergence with global warming levels supports a more policy-relevant communication of the emergence of climate signals given that global policies are very much based on warming levels (e.g., 1.5 or 2.0°C targets of the Paris Agreement). We find that GWLoE provides a feasible tool to constrain model uncertainty, particularly for temperature variables and temperature-related indices. We generally find a higher model agreement for TNx and TXx if emergence is expressed as a function of GWL (Supplementary Fig. S3, S5, S13) instead of time (Supplementary Fig. S4, S6, S14). However, regional differences remain. For PRCPtot and Rx1day, in contrast, we find better agreement across SMILEs when expressing emergence as a function of time. This indicates that precipitation changes are not only impacted by thermodynamics but also by other processes, such as aerosol forcing (Lin et al. 2016; Lehner & Coats 2021), which are characterized as a function of time rather than GWL. In that regard, precipitation changes are more dependent on the scenario pathway and thus more prone to scenario uncertainties in some regions (Maher et al. 2019). Additionally, precipitation changes are more affected by small-scale processes and thus model resolution, which contributes to the larger model spread for precipitation than temperature indices as discussed above.

In particular for the assessment of impacts at low GWLs, i.e., projections of the upcoming decades, internal climate variability is a large source of uncertainty (Hawkins and Sutton 2009, Lehner et al. 2020). Due to their increased sample size, SMILEs allow for a robust signal detection even at these low GWLs (Maher et al. 2020) and thus provide an essential tool to determine GWLoE. Considering the joint emergence of SMILEs allows for a robust assessment of GWLoE and constrains both internal variability and model uncertainty across a wide range of GWLs. Further, the approach considering GWL rather than time to estimate emergence might be beneficial to overcome the "hot model problem" (Hausfather et al. 2022), i.e., the issue of selecting climate models that show a higher-than-average equilibrium climate sensitivity (ECS) to increasing CO_2 levels (Suarez-Gutierrez et al. 2021). We find that a time-dependent approach will generally lead to a model order, where models with high ECS (Tab. 1) usually show the highest exposure of population and land area to emerged climate signals (Supplementary Fig. S4, S6, S14). In contrast, our results show that a GWL-centered analysis results in a model ordering that is largely independent of the models' ECS (Supplementary Fig. S3, S5, S13). This holds particularly true for temperature indices and to a lesser degree also for PRCPtot and Rx1day. In particular for Rx1day model resolution seems to be more impactful than ESC.

Finally, our results are based on the high-end warming scenario SSP5-8.5, which is considered to project a low-probability high warming for the end of the 21st century, given current climate policies (Hausfather & Peters, 2020). Analyzing the impacts of high warming levels (>3.0°C) however, requires the selection of rather extreme warming scenarios (SSP3-7.0 or SSP5-8.5), as these scenarios are the only ones that reach sufficiently high warming (Meinshausen et al. 2020). Furthermore, temperature and precipitation changes were found to scale largely linearly across scenarios for moderate GWLs (Seneviratne et al. 2016) and given that we use a cut-off GWL of 4°C, our results should still be considered robust for the range of GWLs that we investigate.

5 Conclusions

In this study, we present the global warming level of emergence (GWLoE) of four temperature and precipitation indices (TXx, TNx, PRCPtot, and Rx1day) and the related exposure of population and land area based on the joint emergence of five SMILEs. Under current warming levels, large parts of the global population and global land area are already exposed to TXx and TNx emergences, while PRCPtot and Rx1day are about to emerge in several regions. We find widespread emergence of TXx and TNx at a GWL of 2.0°C and linear increases in the emergence of PRCPtot and Rx1day over the GWL range 1.0-2.0°C. Emergences of TXx, PRCPtot, and Rx1day continue increasing beyond 2.0°C. These results confirm that a GWL of 2.0°C should not be misinterpreted as a safe target (Knutti et al. 2016). For higher warming levels (>2.0°C) strong increases in the fraction of exposed land area and population to emerged climate signals were identified for precipitation indices (PRCPtot and Rx1day). Further, we identify a sharp increase in the frequency of temperature extremes (assessed through probability ratios of TXx and TNx) particularly at lower GWLs. These results highlight that considering incremental GWL steps for analyzing the emergence of climate change signals is essential.

Given the dominant role of internal variability at low GWLs that are close to present-day warming we argue that large ensemble simulations are essential. First, to robustly detect the emergence of climate change signals and second, for their assessment at incremental GWL steps, particularly for analyses of extreme events. Using GWLs over time to detect the emergence of climate change signals proofs to be particularly well suited for temperature-based indices. Here, it substantially reduces the uncertainty of signal emergence compared to a time-based approach. For precipitation-based indices we find lower uncertainties when expressing their emergence as a function of time instead of GWL. The decision of whether to apply GWLoE or ToE depends on the considered climate variable and additionally needs to respect regional specifications as indicated by the large regional discrepancy in our results. Further, the strong sensitivity of the emergence of Rx1day on the remapping sequencing highlights the need to tailor the order of remapping to the individual research focus of each study.

Our results underline the importance of climate mitigation and the imminent need for an early achievement of net zero emissions (Iyer et al. 2022) to avoid strongly increasing emergences of temperature and precipitation indices. This urges for the implementation of policies to ensure that global warming is limited at least to the targets defined in the Paris agreement. Every fraction of a degree matters to prevent additionally emerging adverse effects of climate change on human wellbeing.

Acknowledgments

While the presented study originates from a joint hackathon meeting and thus represents a true group effort, the following individual contributions are recognized. D.G. and R.R.W developed the general study concept and all authors contributed to the detailed outline of the study. D.G. contributed with the calculation of the joint GWLoE and drafted the first version of the manuscript. A.B. calculated the probability ratios, drafted the corresponding sections in the manuscript, and produced the presented maps. C.S. provided the GWLs for all SMILEs, performed the exposure analysis, drafted the corresponding section in the manuscript and provided the related figures. M.M. led the SMILE selection process, contributed with coding support and conducted a critical literature screening. M.S. provided the ETCCDI precipitation and temperature indices. All authors actively discussed all results and contributed extensively to

writing the final manuscript. We further acknowledge the World Climate Research Programme, which, through its Working Group on Coupled Modelling, coordinated and promoted CMIP6. We thank the climate modeling groups for producing and making available their model output, the Earth System Grid Federation (ESGF) for archiving the data and providing access, and the multiple funding agencies who support CMIP6 and ESGF.

Open Research

The applied CMIP6 SMILEs with the corresponding variables and projections under historical and SSP5-8.5 scenarios are available under the ESGF nodes (e.g., https://esgf-data.dkrz.de/projects/esgf-dkrz/). Population data can be accessed via https://www.isimip.org/gettingstarted/input-data-bias-adjustment/. All codes to perform the presented analyses and data to derive the respective figures will be shared through a public repository upon publication of the manuscript.

References

Abatzoglou, J. T., Williams, A. P., & Barbero, R. (2019). Global emergence of anthropogenic climate change in fire weather indices. *Geophysical Research Letters*, *46*(1), 326-336.

Ciavarella, A., Cotterill, D., Stott, P. et al. Prolonged Siberian heat of 2020 almost impossible without human influence. Climatic Change 166, 9 (2021). https://doi.org/10.1007/s10584-021-03052-w

Deng, X., Perkins-Kirkpatrick, S. E., Alexander, L. V., & Stark, C. (2022). Projected Changes and Time of Emergence of Temperature Extremes over Australia in CMIP5 and CMIP6. *Earth's Future*, *10*(9), e2021EF002645.

Deser, C., Lehner, F., Rodgers, K. B., Ault, T., Delworth, T. L., DiNezio, P. N., ... & Ting, M. (2020). Insights from Earth system model initial-condition large ensembles and future prospects. *Nature Climate Change*, *10*(4), 277-286.

de Vries, I. E., Sippel, S., Pendergrass, A. G., & Knutti, R. (2023). Robust global detection of forced changes in mean and extreme precipitation despite observational disagreement on the magnitude of change. *Earth System Dynamic*s, 14(1), 81-100

Fischer, E. M., & Knutti, R. (2015). Anthropogenic contribution to global occurrence of heavy-precipitation and high-temperature extremes. *Nature climate change*, *5*(6), 560-564.

Frieler, K., Lange, S., Piontek, F., Reyer, C. P., Schewe, J., Warszawski, L., ... & Yamagata, Y. (2017). Assessing the impacts of 1.5 C global warming–simulation protocol of the Inter-Sectoral Impact Model Intercomparison Project (ISIMIP2b). *Geoscientific Model Development*, *10*(12), 4321-4345.

Gidden, M. J., Riahi, K., Smith, S. J., Fujimori, S., Luderer, G., Kriegler, E., ... & Takahashi, K. (2019). Global emissions pathways under different socioeconomic scenarios for use in CMIP6: a

618 dataset of harmonized emissions trajectories through the end of the century. *Geoscientific model*
619 *development*, 12(4), 1443-1475.

620 Harrington, L. J., & Otto, F. E. (2018). Adapting attribution science to the climate extremes of
621 tomorrow. Environmental Research Letters, 13(12), 123006.

622 Harrington, L. J. (2021). Temperature emergence at decision-relevant scales. Environmental
623 Research Letters, 16(9), 094018.

624 Hauser, M., Engelbrecht, F., & Fischer, E. M.(2019). Transient warming levels for CMIP5 and
625 CMIP6. Zenodo. Available at
626 https://doi.org/10.5281/zenodo.3591807doi:10.5281/zenodo.3591807.

627 Hausfather, Z., Marvel, K., Schmidt, G. A., Nielsen-Gammon, J. W., & Zelinka, M. (2022).
628 Climate simulations: recognize the 'hot model'problem. Nature, 605(7908), 26-29.

629 Hausfather, Z., & Peters, G. P. (2020). Emissions–the 'business as usual'story is
630 misleading. Nature, *577*(7792), 618-620.

631 Hawkins, E., & Sutton, R. (2009). The potential to narrow uncertainty in regional climate
632 predictions. *Bulletin of the American Meteorological Society*, *90*(8), 1095-1108.

633 Hawkins, E., & Sutton, R. (2012). Time of emergence of climate signals. *Geophysical Research*
634 *Letters*, *39*(1).

635 Hawkins, E., Anderson, B., Diffenbaugh, N. et al. Uncertainties in the timing of unprecedented
636 climates. Nature 511, E3–E5 (2014). https://doi.org/10.1038/nature13523

637 Hoegh-Guldberg, O., Jacob, D., Taylor, M., Guillén Bolaños, T., Bindi, M., Brown, S., ... &
638 Zhou, G. (2019). The human imperative of stabilizing global climate change at 1.5
639 C. *Science*, *365*(6459), eaaw6974.

640 IPCC, 2021: Summary for Policymakers. In: Climate Change 2021: The Physical Science Basis.
641 Contribution of Working Group I to the Sixth Assessment Report of the Intergovernmental Panel
642 on Climate Change [Masson-Delmotte, V., P. Zhai, A. Pirani, S.L. Connors, C. Péan, S. Berger,
643 N. Caud, Y. Chen, L. Goldfarb, M.I. Gomis, M. Huang, K. Leitzell, E. Lonnoy, J.B.R. Matthews,
644 T.K. Maycock, T. Waterfield, O. Yelekçi, R. Yu, and B. Zhou (eds.)]. Cambridge University
645 Press, Cambridge, United Kingdom and New York, NY, USA, pp. 3−32,
646 doi:10.1017/9781009157896.001

647 IPCC, 2022: Summary for Policymakers. In: Climate Change 2022: Mittigation of Climate
648 Change. Contribution of Working Group III to the Sixth Assessment Report of the
649 Intergovernmental Panel on Climate Change [P.R. Shukla,J. Skea, R.Slade, A. Al Khourdajie, R.
650 van Diemen, D. McCollum, M. Pathak, S. Some, P. Vyas, R. Fradera, M. Belkacemi, A. Hasija,
651 G. Lisboa, S. Luz, J. Malley, (eds.)]. Cambridge University Press, Cambridge, UK and New
652 York, NY, USA. doi: 10.1017/9781009157926.001Iyer, G., Ou, Y., Edmonds, J., Fawcett, A. A.,
653 Hultman, N., McFarland, J., ... & McJeon, H. (2022). Ratcheting of climate pledges needed to
654 limit peak global warming. Nature Climate Change, 1-7.

Iyer, G., Ou, Y., Edmonds, J., Fawcett, A. A., Hultman, N., McFarland, J., ... & McJeon, H. (2022). Ratcheting of climate pledges needed to limit peak global warming. *Nature Climate Change*, 1-7.

Jones, B., & O'Neill, B. C. (2016). Spatially explicit global population scenarios consistent with the Shared Socioeconomic Pathways. *Environmental Research Letters*, *11*(8), 084003.

Kay, J. E., Deser, C., Phillips, A., Mai, A., Hannay, C., Strand, G., ... & Vertenstein, M. (2015). The Community Earth System Model (CESM) large ensemble project: A community resource for studying climate change in the presence of internal climate variability. *Bulletin of the American Meteorological Society*, *96*(8), 1333-1349.

King, A. D., Donat, M. G., Fischer, E. M., Hawkins, E., Alexander, L. V., Karoly, D. J., ... & Perkins, S. E. (2015). The timing of anthropogenic emergence in simulated climate extremes. *Environmental Research Letters*, *10*(9), 094015.

King, A. D., & Harrington, L. J. (2018). The inequality of climate change from 1.5 to 2 C of global warming. Geophysical Research Letters, 45(10), 5030-5033.

King, A. D., & Karoly, D. J. (2017). Climate extremes in Europe at 1.5 and 2 degrees of global warming. Environmental Research Letters, 12(11), 114031.

King, A. D., Knutti, R., Uhe, P., Mitchell, D. M., Lewis, S. C., Arblaster, J. M. Freychet, N. (2018): On the Linearity of Local and Regional Temperature Changes from 1.5 °C to 2 °C of Global Warming. *Journal of Climate.* 31, 7495 –7514.

Kirchmeier-Young, M. C., Wan, H., Zhang, X., & Seneviratne, S. I. (2019). Importance of framing for extreme event attribution: The role of spatial and temporal scales. *Earth's Future*, *7*(10), 1192-1204.

Knutti, R., Rogelj, J., Sedláček, J., & Fischer, E. M. (2016). A scientific critique of the two-degree climate change target. *Nature Geoscience*, *9*(1), 13-18.

Lehner, F., Coats, S., Stocker, T. F., Pendergrass, A. G., Sanderson, B. M., Raible, C. C., and Smerdon, J. E. (2017a), Projected drought risk in 1.5°C and 2°C warmer climates, *Geophys. Res. Lett.*, 44, 7419– 7428, doi:10.1002/2017GL074117.

Lehner, F., C. Deser, and L. Terray, (2017b), Toward a New Estimate of "Time of Emergence" of Anthropogenic Warming: Insights from Dynamical Adjustment and a Large Initial-Condition Model Ensemble. *J. Climate*, **30**, 7739–7756, https://doi.org/10.1175/JCLI-D-16-0792.1.

Lehner, F., Deser, C., Maher, N., Marotzke, J., Fischer, E. M., Brunner, L., ... & Hawkins, E. (2020). Partitioning climate projection uncertainty with multiple large ensembles and CMIP5/6. *Earth System Dynamics*, *11*(2), 491-508.

Lehner, F., & Coats, S. (2021). Does regional hydroclimate change scale linearly with global warming?. Geophysical Research Letters, 48(23), e2021GL095127.

690 Lehner, F., Hawkins, E., Sutton, R., Pendergrass, A. G., & Moore, F. C. (2023). New Potential to
691 Reduce Uncertainty in Regional Climate Projections by Combining Physical and Socio-
692 Economic Constraints. *AGU Advances*, *4*(4), e2023AV000887.

693 Lenton, T. M., Xu, C., Abrams, J. F., Ghadiali, A., Loriani, S., Sakschewski, B., ... & Scheffer,
694 M. (2023). Quantifying the human cost of global warming. Nature Sustainability, 1-11.

695 Lin, L., Wang, Z., Xu, Y., & Fu, Q. (2016). Sensitivity of precipitation extremes to radiative
696 forcing of greenhouse gases and aerosols. Geophysical Research Letters, 43, 9860–9868.

697 Liu, P. R., & Raftery, A. E. (2021). Country-based rate of emissions reductions should increase
698 by 80% beyond nationally determined contributions to meet the 2 C target. Communications
699 earth & environment, 2(1), 29.

700 Mackallah, C, Chamberlain, M. A., Law, R. M., Dix, M., Ziehn, T., Bi, D., ... & Yeung, N.
701 (2022). ACCESS datasets for CMIP6: methodology and idealised experiments. *Journal of*
702 *Southern Hemisphere Earth Systems Science*, *72*(2), 93-116.

703 Maher, N., Milinski, S., Suarez-Gutierrez, L., Botzet, M., Dobrynin, M., Kornblueh, L., ... &
704 Marotzke, J. (2019). The Max Planck Institute Grand Ensemble: enabling the exploration of
705 climate system variability. *Journal of Advances in Modeling Earth Systems*, *11*(7), 2050-2069.

706 Maher, N., Lehner, F., & Marotzke, J. (2020). Quantifying the role of internal variability in the
707 temperature we expect to observe in the coming decades, Environmental Research Lettters,
708 15(5), 10.1088/1748-9326/ab7d02

709 Maher, N., Milinski, S., & Ludwig, R. (2021a). Large ensemble climate model simulations:
710 introduction, overview, and future prospects for utilising multiple types of large ensemble. *Earth*
711 *System Dynamics*, *12*(2), 401-418.

712 Mahlstein, I., Hegerl, G., & Solomon, S. (2012). Emerging local warming signals in
713 observational data. *Geophysical Research Letters*, *39*(21).

714 Martel, J. L., Mailhot, A., Brissette, F., & Caya, D. (2018). Role of natural climate variability in
715 the detection of anthropogenic climate change signal for mean and extreme precipitation at local
716 and regional scales. *Journal of Climate*, *31*(11), 4241-4263.

717 Masson-Delmotte, V., Zhai, P., Pörtner, H. O., Roberts, D., Skea, J., Shukla, P. R., ... &
718 Waterfield, T. (2018). Global warming of 1.5 C. *An IPCC Special Report on the impacts of*
719 *global warming of*, *1*(5)

720 Masson-Delmotte, V., Zhai, P., Pirani, A., Connors, S. L., Péan, C., Berger, S., ... & Zhou, B.
721 (2021). Climate change 2021: the physical science basis. *Contribution of working group I to the*
722 *sixth assessment report of the intergovernmental panel on climate change*, *2*.

723 Mauritsen, T., Bader, J., Becker, T., Behrens, J., Bittner, M., Brokopf, R., ... & Roeckner, E.
724 (2019). Developments in the MPI-M Earth System Model version 1.2 (MPI-ESM1. 2) and its
725 response to increasing CO2. Journal of Advances in Modeling Earth Systems, 11(4), 998-1038.

Meehl, G. A., Senior, C. A., Eyring, V., Flato, G., Lamarque, J. F., Stouffer, R. J., ... & Schlund, M. (2020). Context for interpreting equilibrium climate sensitivity and transient climate response from the CMIP6 Earth system models. *Science Advances*, *6*(26), eaba1981.

Meinshausen, M., Nicholls, Z. R., Lewis, J., Gidden, M. J., Vogel, E., Freund, M., ... & Wang, R. H. (2020). The shared socio-economic pathway (SSP) greenhouse gas concentrations and their extensions to 2500. *Geoscientific Model Development*, *13*(8), 3571-3605.

Milinski, S., Maher, N., and Olonscheck, D.: How large does a large ensemble need to be?, Earth Syst. Dynam., 11, 885–901, https://doi.org/10.5194/esd-11-885-2020, 2020.

Morice, C. P., Kennedy, J. J., Rayner, N. A., Winn, J. P., Hogan, E., Killick, R. E., ... & Simpson, I. R. (2021). An updated assessment of near-surface temperature change from 1850: The HadCRUT5 data set. *Journal of Geophysical Research: Atmospheres*, 126(3), e2019JD032361.

Park, C. E., Jeong, S. J., Joshi, M., Osborn, T. J., Ho, C. H., Piao, S., ... & Feng, S. (2018). Keeping global warming within 1.5 C constrains emergence of aridification. *Nature Climate Change*, *8*(1), 70-74.

Perkins-Kirkpatrick, S. E., Gibson, P. B. (2017): Changes in regional heatwave characteristics as a function of increaseing global temperature. *Scientific Reports*. 7:12256.

Philip, S. Y., Kew, S. F., van Oldenborgh, G. J., Anslow, F. S., Seneviratne, S. I., Vautard, R., Coumou, D., Ebi, K. L., Arrighi, J., Singh, R., van Aalst, M., Pereira Marghidan, C., Wehner, M., Yang, W., Li, S., Schumacher, D. L., Hauser, M., Bonnet, R., Luu, L. N., Lehner, F., Gillett, N., Tradowsky, J. S., Vecchi, G. A., Rodell, C., Stull, R. B., Howard, R., and Otto, F. E. L.: Rapid attribution analysis of the extraordinary heat wave on the Pacific coast of the US and Canada in June 2021, Earth Syst. Dynam., 13, 1689–1713, https://doi.org/10.5194/esd-13-1689-2022, 2022.

Philip, S., Kew, S., Vautard, R., Vahlberg, M., Singh, R., Driouech, F., ... & Otto, F. (2023). Extreme April heat in Spain, Portugal, Morocco & Algeria almost impossible without climate change.

Raymond, C., Matthews, T., & Horton, R. M. (2020). The emergence of heat and humidity too severe for human tolerance. *Science Advances*, *6*(19), eaaw1838.

Royé, D., Sera, F., Tobías, A., Lowe, R., Gasparrini, A., Pascal, M., de'Donato, F., Nunes, B., and Teixeira, J. P.: Effects of Hot Nights on Mortality in Southern Europe, Epidemiology, 32, 487–498, https://doi.org/10.1097/EDE.0000000000001359, 2021.

Samir, K. C., & Lutz, W. (2017). The human core of the shared socioeconomic pathways: Population scenarios by age, sex and level of education for all countries to 2100. *Global Environmental Change*, *42*, 181-192.

Schleussner, C.-F., Lissner, T. K., Fischer, E. M., Wohland, J., Perrette, M., Golly, A., Rogelj, J., Childers, K., Schewe, J., Frieler, K., Mengel, M., Hare, W., and Schaeffer, M.: Differential

763 climate impacts for policy-relevant limits to global warming: the case of 1.5 °C and 2 °C, Earth
764 Syst. Dynam., 7, 327–351, https://doi.org/10.5194/esd-7-327-2016, 2016.

765 Schlunegger, S., Rodgers, K. B., Sarmiento, J. L., Frölicher, T. L., Dunne, J. P., Ishii, M., &
766 Slater, R. (2019). Emergence of anthropogenic signals in the ocean carbon cycle. *Nature climate*
767 *change*, *9*(9), 719-725.

768 Schwingshackl, C., Sillmann, J., Vicedo-Cabrera, A. M., Sandstad, M., & Aunan, K. (2021).
769 Heat stress indicators in CMIP6: estimating future trends and exceedances of impact-relevant
770 thresholds. *Earth's Future*, *9*(3), e2020EF001885.

771 Seneviratne, S. I., Donat, M. G., Pitman, A. J., Knutti, R., & Wilby, R. L. (2016). Allowable
772 CO2 emissions based on regional and impact-related climate targets. *Nature*, *529*(7587), 477-
773 483.

774 Seneviratne, S.I., X. Zhang, M. Adnan, W. Badi, C. Dereczynski, A. Di Luca, S. Ghosh, I.
775 Iskandar, J. Kossin, S. Lewis,F. Otto, I. Pinto, M. Satoh, S.M. Vicente-Serrano, M. Wehner, and
776 B. Zhou,2021: Weather and Climate Extreme Events in a Changing Climate. In Climate Change
777 2021: The Physical Science Basis. Contribution of Working Group I to the Sixth Assessment
778 Report of the Intergovernmental Panel on Climate Change [Masson-Delmotte, V., P. Zhai, A.
779 Pirani, S.L. Connors, C. Péan, S. Berger, N. Caud, Y. Chen, L. Goldfarb, M.I. Gomis, M. Huang,
780 K. Leitzell, E. Lonnoy, J.B.R. Matthews, T.K. Maycock, T. Waterfield, O. Yelekçi, R. Yu, and
781 B. Zhou (eds.)]. Cambridge University Press, Cambridge, United Kingdom and New York, NY,
782 USA, pp. 1513–1766, doi:10.1017/9781009157896.013
783
784 Sillmann, J., Kharin, V. V., Zwiers, F. W., Zhang, X., & Bronaugh, D. (2013). Climate extremes
785 indices in the CMIP5 multimodel ensemble: Part 2. Future climate projections. Journal of
786 geophysical research: atmospheres, 118(6), 2473-2493.

787 Suarez-Gutierrez, L., Müller, W. A., Li, C., & Marotzke, J. (2020). Hotspots of extreme heat
788 under global warming. *Climate Dynamics*, *55*(3), 429-447.

789 Suarez-Gutierrez, L., Milinski, S., & Maher, N. (2021). Exploiting large ensembles for a better
790 yet simpler climate model evaluation. Climate Dynamics, 57(9-10), 2557-2580.

791 Swart, N. C., Cole, J. N., Kharin, V. V., Lazare, M., Scinocca, J. F., Gillett, N. P., ... & Winter,
792 B. (2019). The Canadian earth system model version 5 (CanESM5. 0.3). *Geoscientific Model*
793 *Development*, *12*(11), 4823-4873.

794 Tatebe, H., Ogura, T., Nitta, T., Komuro, Y., Ogochi, K., Takemura, T., ... & Kimoto, M. (2019).
795 Description and basic evaluation of simulated mean state, internal variability, and climate
796 sensitivity in MIROC6. *Geoscientific Model Development*, *12*(7), 2727-2765.

797 Tebaldi, C., Debeire, K., Eyring, V., Fischer, E., Fyfe, J., Friedlingstein, P., ... & Ziehn, T.
798 (2021). Climate model projections from the scenario model intercomparison project
799 (ScenarioMIP) of CMIP6. *Earth Syst. Dyn.,* 12(1), 253-293

800 Thompson, R., Landeg, O., Kar-Purkayastha, I., Hajat, S., Kovats, S., and O'Connell, E.:
801 Heatwave Mortality in Summer 2020 in England: An Observational Study, Int. J. Environ. Res.
802 Public. Health, 19, 6123, https://doi.org/10.3390/ijerph19106123, 2022.

803 UNFCCC (2015). Adoption of the Paris Agreement. Report No. FCCC/CP/2015/L.9/Rev.1,
804 http://unfccc.int/resource/docs/2015/cop21/eng/l09r01.pdf.

805 Wood, R. R., Lehner, F., Pendergrass, A. G., & Schlunegger, S. (2021). Changes in precipitation
806 variability across time scales in multiple global climate model large ensembles. *Environmental*
807 *Research Letters*, *16*(8), 084022.

808 Wyser, K., Koenigk, T., Fladrich, U., Fuentes-Franco, R., Karami, M. P., & Kruschke, T. (2021).
809 The SMHI large ensemble (SMHI-lens) with EC-Earth3. 3.1. *Geoscientific Model*
810 *Development*, *14*(7), 4781-4796.